LED SYSTEM WITH INDEPENDENT RED AND BLUE CHANNELS EMPLOYING RADIANT FLUX ESTIMATION AND INDIRECT FLUX CONTROL FOR GREENHOUSE HOP CULTIVATION

P. L. Tavares[1], I. A. B. Guimarães[1], H. A. C. Braga[1],V. C. Bender[2], P. S. Almeida[1]
[1]Federal University of Juiz de Fora – Minas Gerais, Brazil
[2]Federal University of Pampa – Rio Grande do Sul, Brazil
Modern Lighting Research Group – NIMO
E-mail: pedro.laguardia@engenharia.ufjf.br, pedro.almeida@ufjf.edu.br

Abstract – Hops are quite susceptible to weather and radiation. As such, it is a complex task to cultivate hops out of its natural habitats, in low latitude outdoor locations. This paper proposes an indoor alternative to cultivating hops on a small scale for brewery applications, employing a two-channel LED lighting system. Its main component is a driver for a specific R+B LED load, which controls the radiant flux of both red (R) and blue (B) LED strings independently. This LED array was developed specifically to meet the hops' lighting needs, and its photo-electro-thermal (PET) model is considered to estimate and control precisely each of the radiant fluxes emitted in real time. The driver and R+B LED array are used inside the greenhouse which guarantees the adequacy of other abiotic parameters for the crop. An experimental routine is proposed and underway for comparative results between the proposed LED versus conventional fluorescent lighting for growing hops under same environmental conditions.

Keywords **– Light emitting diodes, artificial lighting, LED drivers, photo-electro-thermal model.**

I. INTRODUCTION

Hops (*Humulus lupulus* L.) are plants from the *Cannabaceae* family, essentially employed since the Middle Ages on the process of making beer, i.e., brewing. Its cones (female inflorescences) contain the resin lupulin. Lupulin is made of many acids and essential oils which are elementary ingredients for giving bitterness and aromatic qualities in beer [1]. The increase of beer production on industrial and artisanal (craft) scales implied in a rise for demand of hop cones in countries that do not necessarily have suitable outdoor characteristics for growing these crops [1], [2]. Therefore, the creation of a feasible small scale system for indoor cultivation is something very attractive for local markets since it avoids importation fees and increases the crop stability as a product, while also avoiding degradations from storage and transportation processes, known to reduce significantly the acid concentration of the final product [3].

In this context, this work proposes an alternative way to cultivate hops under indoor (greenhouse) conditions, controlling temperature, atmosphere and solo humidity, O_2/CO_2 concentrations and – most importantly, the radiant flux incident on the plants, which is the main topic of interest in this paper. The experiment underway involves nine hop clones that are divided in groups of three plants, for three lighting environments: under natural light (outdoor control experiment; no management on lighting quality or spectrum), under conventional fluorescent lamps (indoor control experiment, only discontinuous, i.e., ON-OFF control of lighting) and under an R+B LED array (indoor experiment itself; allowing control over lighting spectrum and continuous control on light intensity, i.e., dimming) (Fig. 1).

In order to control the radiant flux for the three plants under LED lighting, a two-channel driver circuit is on development to feed an array of 54 red LEDs (R-channel) plus an array of 18 blue LEDs (B-channel). Both color arrays fed separately, so that, the amount of red and blue light can be adjusted in real time for the appropriate spectrum and R:B ratio at different stages of growth, as well as the intensity of radiant power emitted by each channel.

On the other hand, one of the control experiments – the indoor setup with fluorescent lamps (FL) – has the inherent constraint that the spectrum cannot be manipulated, and the only means of controlling photoperiod is by turning the lights on or off (non-dimmable ballasts). As consequence, in this setup, intensity cannot be seamlessly controlled nor spectrum. On the other hand, their resulting maximum irradiance on the plants' workig plane (measured in W/m² or µmol/m².s) should be compatible with that resulting from the use of the LED arrays – on the other side of the experiment.

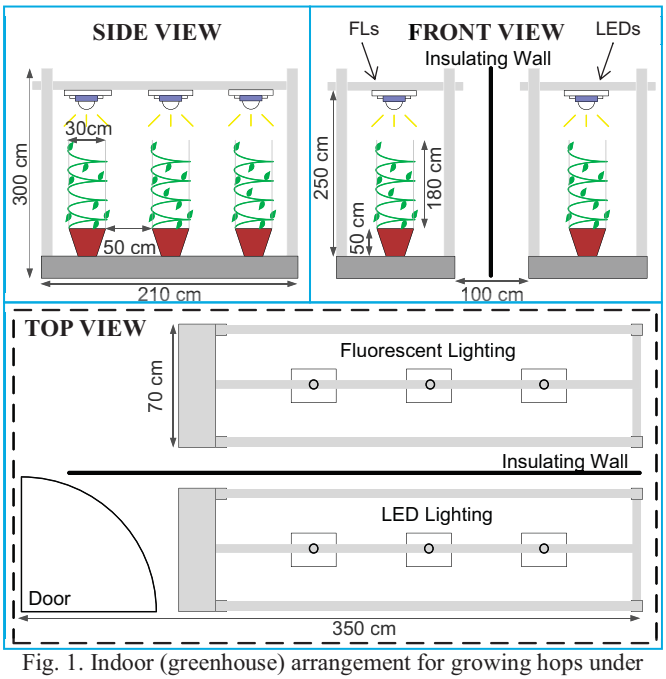

Fig. 1. Indoor (greenhouse) arrangement for growing hops under fluorescent lamps (FL) and LED lighting. Florescent lamps are used as a control experiment, since they are employed as the conventional technology in many greenhouses.

978-1-5090-6248-5/17/$31.00 ©2017 IEEE

This paper is organized as follows: hops characteristics and the lighting effects on its growth and flowering are given in Section II; the photo-electro-thermal (PET) characterization of the LED arrangement for radiant flux estimation is given in Section III; the proposal of a driver topology including a flux estimator and control system are presented in Section IV.

II. HOPS AND CONSIDERATIONS ON ARTIFICIAL LIGHTING FOR PLANT GROWTH

A. General Hops Characteristics

Hops are herbaceous, perennial and long-lived climbing plants from the *Cannabaceae* family, being usually cultivated for its dried female strobiles (cones or flowers) [1], [4]. The strobiles contain in their resin substances called alpha (α) acids (the main of which is humulone), the components responsible for bitterness in beer (in their isomerized form – e.g., isohumulone). The iso-α acids are also used for their bacteriostatic properties that prevent major wort/beer contamination from Gram-positive bacteria and consequent beer spoilage. Currently, the α acid concentration is the main measure used to describe hop crop yield [3]. The concentration of these compounds is largely dependent on the cultivar and on environmental conditions, varying greatly from as low as 2% to as high as 20% by dry weight [6].

The hop plant is native to places of higher latitudes (temperate zones) of Northern Hemisphere, presenting better growth responses in places that share temperature profile and photoperiodic regime of 35th to 50th northern or southern parallels [5]. Therefore, a successful cultivation depends largely on emulating these abiotic conditions of temperature, radiation, water and soil nutrients at indoor environment [7].

B. Photoperiod as a Key Aspect on Plant Cultivation

The hop plant photoperiod has a very important role on growth and flowering induction [1], [4]. As short-day-plants (SDP) [1], they need a long period of uninterrupted darkness for flowering and not necessarily uninterrupted light during daylight emulation. This is convenient on indoor systems, as it can present interruptions on lighting due to power supply disturbances and the plant health will not be compromised [8]. Studies point out that, in the growth (vegetative) stage, the optimal photoperiod regime for hops is 16 hours day-length [1] [4]. These aspects highlight the need of a photoperiod control in the LED driving system to emulate different photoperiod regimes for different plant stages of development (e.g., vegetative vs. flowering). In addition, the different stages of growth and the flowering period require different radiation levels, thus, the driver should be dimmable to control the adequate irradiance in these conditions while maintaining the most efficient spectrum.

C. Light Spectrum Considerations

The spectrum distribution is another fact that has large influence on plants [8]. The maximum areas of absorption in chlorophyll-bearing leaves are close to 432 nm (blue) and 670 nm (red) [7]; this is, in fact, what makes leaves look green. Thus, a source of light focusing on emitting around optimal absorbance implies in more efficacy per electric power dedicated. Studies point out that the lowest price per mol/m² dedicated to the plant can be reached with a combination of red and blue light [9] [10], which correspond to the peaks in leaf chlorophyll absorbance. Fig. 2 shows the absorbance curves of the pigments involved in the photosynthetic process (chlorophyll-a, chlorophyll-b and carotenoids) with its respective compounding (sum) and compares it with the curve traced from data extracted experimentally from a leaf of *H. lupulus* 'Columbus' (a high-alpha hop cultivar) in the Laboratory of Plant Physiology from the Federal University of Juiz de Fora (UFJF).

As shown in Fig. 2, the absorption peaks from measured data were at 442 nm and 674 nm. The curve profile is fairly close to the one found in the literature due to the fact that the pigments contents are similar among all higher plants [8].

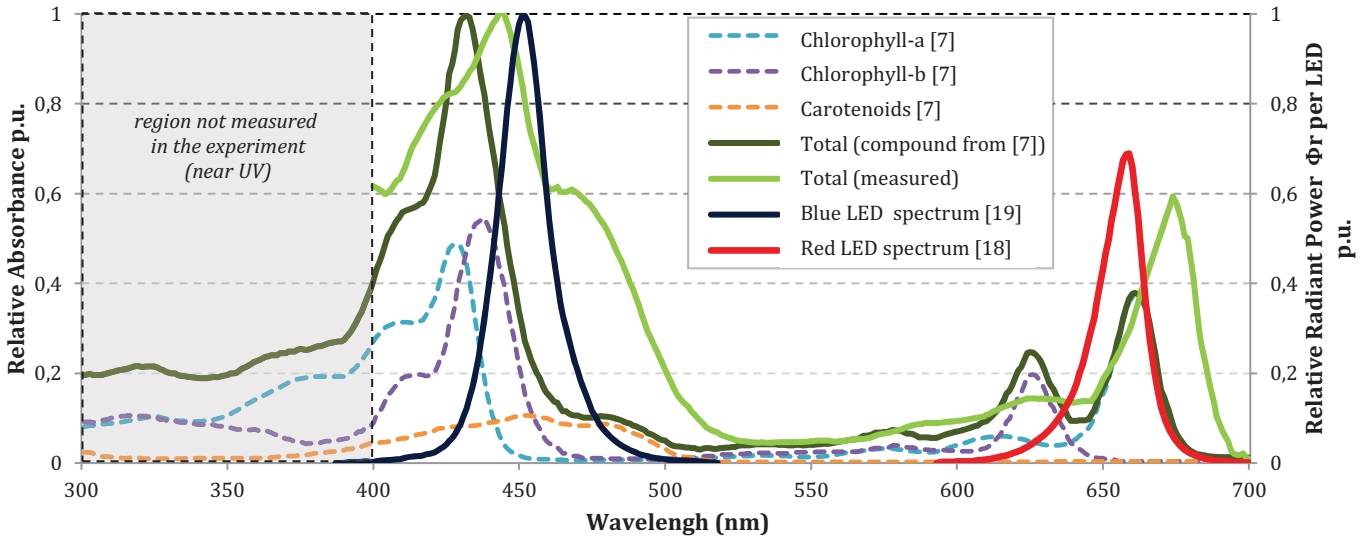

Fig. 2. Comparison among relative absorbance of chlorophylls a, b and carotenoids, by reference [7], along with relative absorbance measured at the laboratory for a Columbus hop leaf. Also shown are the relative spectral power distributions (SPD) of both the selected red and blue LEDs (both LED SPDs are normalized to the blue LED's peak emission value, which is the highest amongst the two).

Although short wavelengths present higher absorbance on the graph, the photosynthetic efficiency is not simply related to absorbance. Shorter wavelength photons also have more energy than longer wavelength photons; consequently, the short wavelength presents a large portion of energy absorbance on the graph, but not the majority of photons related to photosynthesis. In fact, most plants tend to use red light best because of the higher quantum yield radiation centered on 620 nm [11] – blue (440 nm) radiation presents, on average, 70% of the quantum yield of red. The spectrum balance (i.e., amount of each color) is also a strongly affecting factor, being susceptible to change on its optimal distribution according to the plant growth stage [9], [11].

Researchers highlight some spectrum ratios of red and blue light depending on the type of plant and crop objective (fruiting, inflorescences or biomass), with red light usually dominating the spectrum [11], [12], [13]; this is why many grow lights appear pinkish. In accordance to this premise taken from literature, this experiment proposes a proportion of 2:1 red to blue (R:B) in maximum radiant power ratio, which corresponds approximately to the Sunlight Spectral Power Distribution (SPD) proportion at 37º latitude [14].

It is important to remark that, due to the nature of the driver on development, the R:B ratio does not need to be fixed at this 2:1 value; the two independently-dimmable channels in the driver allow for adjustments during the cultivation process to analyze and target optimal spectrum balance for hop growth and flowering stages. Therefore, this R:B ratio can be altered in real time and continuously adjusted – along with photoperiod – for each growth phase.

III. LED ARRANGEMENT AND PET MODEL

A. LED Arrangement – The "LED Lamp"

The LEDs chosen for the prototype were the OSLON SSL 120 type, models GH CSSPM1.24 "hyper red" [20] and GD CSSPM1.14 "deep blue" [21], both manufactured by OSRAM Opto Semiconductors. These models were chosen according to the previous analysis on chlorophyll pigments' peak absorbance (Fig. 2) and LED availability in the market. Both LEDs' spectra are presented together in the same Fig. 2, their spectra being normalized to the peak emission of the most energetic and efficient one (deep blue LED).

The two-channel arrangement is thus composed of an array of 54 hyper red (660 nm, 425 mW @ 350 mA) LEDs – the R-channel – plus an array of 18 deep blue (451 nm, 690 mW @ 350 mA) LEDs – the B-channel. At a maximum design current chosen at 500 mA, for both (the LEDs in each string are series-associated), the R-channel totals a maximum of 60 W electric power and 34 W of radiant power (at η_R = 56% radiant efficiency [20]), whereas the B-channel totals a maximum of 26 W electric power and 18 W of radiant power (at η_B = 69% radiant efficiency [21]). This corresponds roughly to a 2:1 ratio on radiant flux (Φ_R:Φ_B) when both channels are driven under maximum power (86 W in total), although the ratio in the actual number of LEDs is 3:1 (n_R:n_B). The ratios Φ_R:Φ_B and n_R:n_B differ because of the different forward voltages of the red and blue LEDs (which affect electrical power) and their different radiant efficiencies.

It was found that 54+18 R+B LEDs would meet the demand of the three adult hop plants above their photosynthesis compensation point not compromising the plants yields [15]. The luminaire totalizes 52 W radiant power; this corresponds to 18+6 of R+B LEDs for each of the plants – or roughly 17 W of total radiant power per plant.

This LED arrangement being built (the "LED lamp") is illustrated on Fig. 3 for the total 54 hyper red and 18 deep blue LEDs. They are clustered in 4-LED "blocks" (3 red, 1 blue), six of whom form a "module". The "blocks" are devised in a way to keep the uniformity of irradiance field and to realize physical spectrum mixing. All the LEDs share the same heatsink and all the components of each channel are connected in series, as indicated in Fig. 3. Each of the so-called "modules" – clusters of 6 "blocks", though not independent from each other (their channels are cascaded to the following "module" and they all sit at the same heatsink), should be responsible for the illumination of one plant.

B. LED Characteristics and PET Model of the Arrangement

The LED spectrum and relevant radiometric parameters such as radiant flux (Φ_x), among others, are dependent on thermal and electrical parameters [16], [17]. The photo-electro-thermal (PET) model links these three factors in a way to estimate the LED radiant flux and visualize possible optimal operating points and designs [16]. It is not only a useful tool for system-oriented design, but also provides the mathematical framework for radiant flux estimation in each of the channels of the proposed two-channel LED system. By measuring electrical parameters (voltage and current), one can estimate flux and thus indirectly control it.

This section uses the static PET analysis proposed by [18] and [19] to provide a mathematical model for both the LED channels used on this work, leading to equations that will be used in the flux estimation and control of both of the LED driver channels.

Fig. 4 gives the equivalent thermal circuit of the R and B-channels sitting in the same heatsink considering the dependence of LED voltage on junction temperature (represented by the temperature-controlled voltage source). The thermal circuit is shown explicitly only for the R-channel, but it is the same topology for the B-channel, varying only on its parameters.

The parameters of R and B channels are, respectively: V_R and V_B are the terminal voltages of the whole channel. I_R and I_B are the currents through each LED channel, n_R and n_B are the number of LEDs in series in each channel (n_R = 54; n_B = 18 according to the previous design).

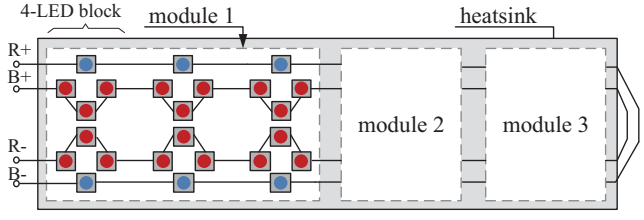

Fig. 3. The 54+18 R+B LED arrangement ("lamp"), designed for three plants. All the so-called "modules" are identical, comprising 2 channels (R and B) each, with all the LEDs in each channel connected in series and both channels sharing a common heatsink.

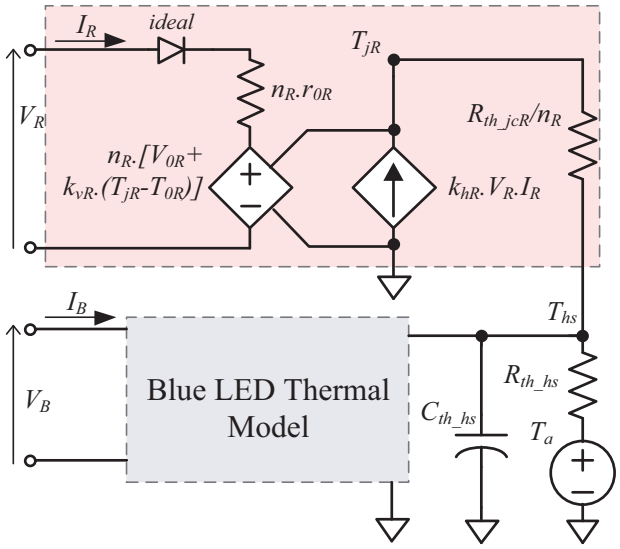

Fig. 4. Equivalent thermal circuit of Blue and Red LED channels.

r_{0R} and r_{0B} are the equivalent series resistances of each single LED. V_{0R} and V_{0B} are the threshold ("knee") voltage of each single LED. k_{vR} and k_{vB} are the coefficients of LED forward voltage change with temperature (these are known to be negative [19]). k_{hR} and k_{hB} are coefficients of conversion from electric power to thermal power (i.e., the complement of radiant efficiency of each LED: $k_{hx} = 1 - \eta_x$), which give the amount of heat each LED produces at a given power. R_{th_jcR} and R_{th_jcB} are the junction-to-case thermal resistances of each single LED. T_{jR} and T_{jB} are the junction temperatures of each single LED (assumed equal for all LEDs of the same type – R or B). R_{th_hs} is the thermal resistance of the whole heatsink. T_{hs} is the heatsink temperature. C_{th_hs} is the thermal capacitance of the whole heatsink. T_a is ambient temperature. T_{0R} and T_{0B} are the test temperatures of each device (as given by manufacturer; $T_{0R} = T_{0B} = 25$º C for both LEDs employed). I_{0R} and I_{0B} are the test currents of each device (also as given by manufacturer. $I_{0R} = I_{0B} = 350$ mA for both LEDs employed). Manufacturer also gives the rated (nominal) radiant fluxes (Φ_{0x}) of each single LED: $\Phi_{0R} = 425$ mW @ $I_{0R} = 350$ mA / $T_{0R} = 25$º C and $\Phi_{0B} = 690$ mW @ $I_{0B} = 350$ mA / $T_{0B} = 25$º C – all info from [20], [21].

Consider that "x" denotes either "R" when regarding the R-channel or "B" for the B-channel in the following equations, for brevity, since both electro-thermal circuits are identical, only differing in their parameter values.

Equation (1) expresses the terminal voltage of a channel according to the piecewise temperature-dependent linear model of each LED array and its circuit showed on Fig. 4 [18]. One can notice that the terminal voltage is related to the change in junction temperature $(T_{jx} - T_{0x})$, thus can be utilized to estimate this temperature if the current I_x is also known. This relation is expressed in (2) – directly obtained from isolating T_{jx} in (1) and making it a function of V_x and I_x.

$$V_x\left(I_x, T_{jx}\right) = n_x\left[r_{0x} I_x + V_{0x} + k_{vx}\left(T_{jx} - T_{0x}\right)\right] \quad (1)$$

$$T_{jx}\left(V_x, I_x\right) = \frac{V_x / n_x - r_{0x} I_x - V_{0x}}{k_{vx}} + T_{0x} \quad (2)$$

where the subscript x indicates either the red (R) or blue (B) channel or LED.

The equation which bonds the thermal and electrical operating points of each channel of the system to its respective resulting total radiant flux (Φ_x) is show in (3) [19]:

$$\Phi_x\left(I_x, T_{jx}\right) = n_x \Phi_{0x}\left(d_{0x} + d_{1x} I_x\right)\left(c_{0x} + c_{1x} T_{jx}\right) \quad (3)$$

In the PET modeling, Φ_{0x} is the nominal (rated) flux given by manufacturer at test current (I_{0x}) and test junction temperature (T_{jx}). The manufacturer also provides other two essential normalized curves for photometric behavior: a) how flux changes with current under constant temperature ($T_{jx} = T_{0x}$) and b) how it changes with junction temperature under constant current ($I_x = I_{0x}$). Both curves are essentially lines; thus, d_{0x} and c_{0x} are the linear coefficients of the first (Φ_x vs. I_x) and second (Φ_x vs. T_{jx}) curves, respectively whereas d_{1x} and c_{1x} are their respective angular coefficients. It is known that d_{0x} is close to zero and that d_{1x} is a positive coefficient whereas c_{1x} is a negative coefficient, because flux increases with current but decreases with temperature. It is obvious from (3) that in the condition $I_x = I_{0x}$ and $T_{jx} = T_{0x}$, flux will be $\Phi_x = n_x \Phi_{0x}$ for each of the (whole) channels.

The descriptions given in equations (2) and (3) embody how a simple flux estimator for each of the channels can be achieved: if the terminal voltage and current of both R and B-channels (V_R, V_B, I_R, I_B) are measured, then by knowing all the parameters that appear in (2) and (3) (Φ_{0x}, T_{0x}, V_{0x}, r_{0x}, k_{vx}, c_{0x}, c_{1x}, d_{0x}, d_{1x}), for each of the LED types, and the number of LEDs in each array (n_R, n_B), the junction temperature in each LED (T_{jx}) can be estimated from (2) and, then, (3) can be applied to calculate the total radiant flux of each channel, without any knowledge of the thermal circuit parameters themselves and without resorting to temperature measurements. Thus, the flux estimator consists of a temperature junction estimator plus a flux calculation, (3).

Fig. 5 shows four graphs which corresponds to the four main characteristic curves of both LED models used in the arrangement. The graphs were traced from the curves given in the datasheets through digitalization of their points (two curves in each graph). To extrapolate the curves and obtain the constants of the PET model, the least squares method was adopted, finding the parameters: V_{0R}, r_{0R} and V_{0B}, r_{0B} from Fig. 5(a) – electrical interaction; d_{0R}, d_{1R} and d_{0B}, d_{1B} from Fig. 5(b) – photo-electrical interaction; c_{0R}, c_{1R} and c_{0B}, c_{1B} from Fig. 5(c) – photo-thermal interaction; and finally k_{vR} and k_{vB} from Fig. 5(d) – electro-thermal interaction. As a remark, data points for temperatures below 25º C were not considered on the extrapolations done. These are in Table I.

TABLE I
Parameters found from Extrapolated Data for both LEDs

Parameter	Red LED	Blue LED
V_{0x}	1.792 V	2.715 V
r_{0x}	0.855 Ω	0.352 Ω
d_{0x}	0.062	0.249
d_{1x}	2.623 A^{-1}	2.072 A^{-1}
c_{0x}	1.068	1.03
c_{1x}	-1.834×10^{-3} º C^{-1}	-0.899×10^{-3} º C^{-1}
k_{vx}	-1.347×10^{-3} V º C^{-1}	-1.441×10^{-3} V º C^{-1}

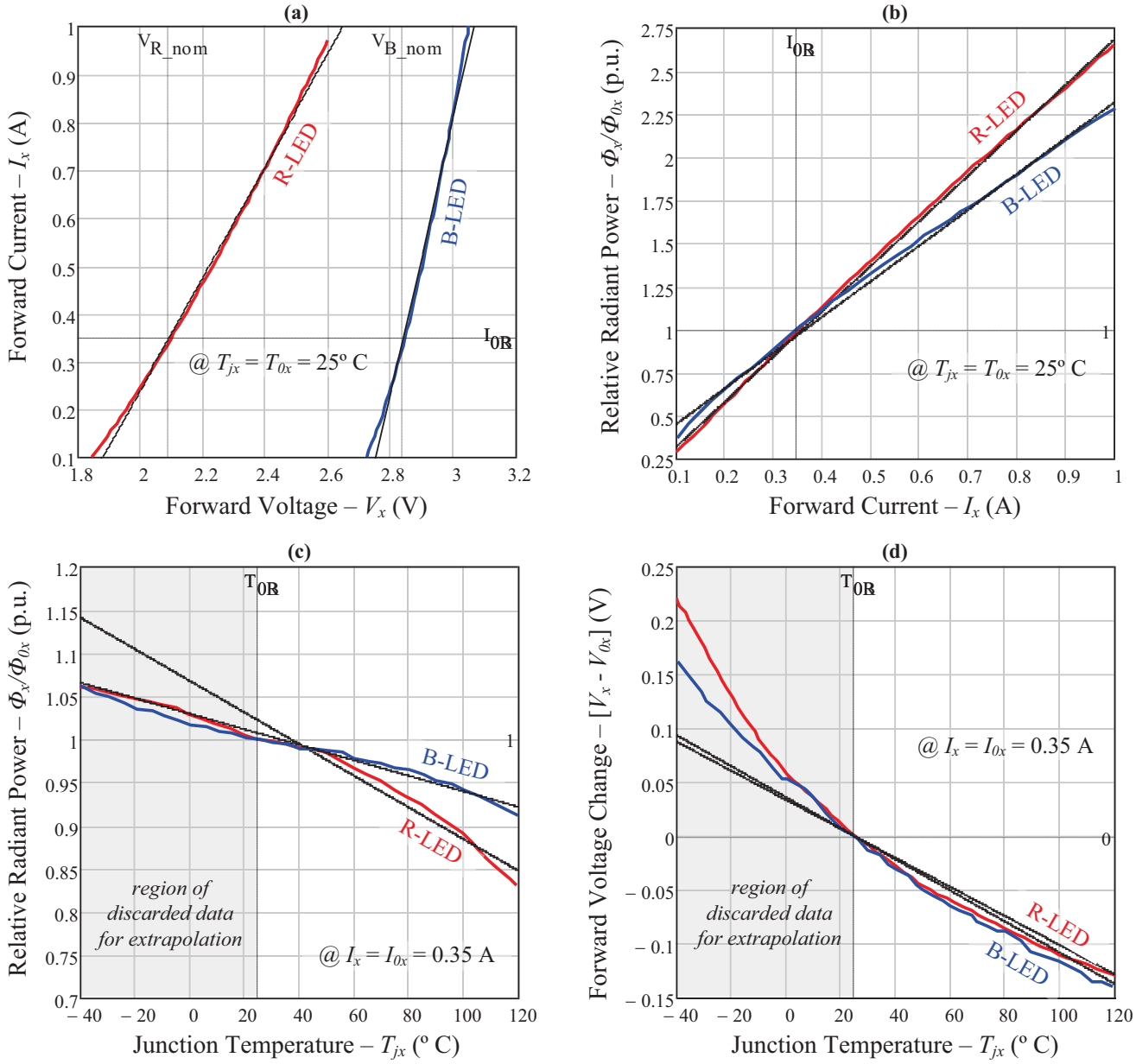

Fig. 5. Characteristic curves of both LEDs, from [20] and [21], plus their linear extrapolations: (a) current versus voltage, (b) normalized radiant flux versus current, (c) normalized radiant flux versus junction temperature and (d) change in voltage versus change in temperature. The four extrapolated curves for each of the LEDs (eight in total) are the solid black lines superimposed to the original (colored) curves.

IV. A TWO-CHANNEL DRIVER WITH INDIRECT FLUX ESTIMATION AND CONTROL

A. Overall Driver Topology

The two-channel driver being built is the main part of the experimental greenhouse system. The driver has some desirable characteristics, the main of which are: a) the ability to drive both channels (R and B) independently, with dimming control on each; b) operating from mains voltage, with high power factor; c) controlling indirectly the radiant flux of each LED channel by using electro-thermal estimation of radiant flux and a flux control whose reference can be given externally. An overall topology of such a driver is given in Fig. 6. In this figure, the lower-case variables (i_x, v_x) denote the instantaneous electrical values and the asterisk denotes control references (set points).

As seen in Fig. 6, one of the most vital characteristics of the electronic driver under development – the indirect and independent flux control on each channel – is actually a current control: an inner current loop, which is acted upon on its current reference by the flux estimator and the outer flux control loop. The flux estimation on each channel is to be compared to the actual flux references (given externally by the experimentalist or by a supervisory system that continuously commands the emulation of the desired spectrum and photoperiod), and the compensated flux errors are used as current references for the inner current control loops. As an advantage of this system, only electrical parameters are to be measured (neither photometrical nor thermal): each of the channels currents (I_R, I_B) and voltages (V_R, V_B); I_x and V_x are used to estimate the x-channel flux, whereas I_x is also used in the respective channel current loop.

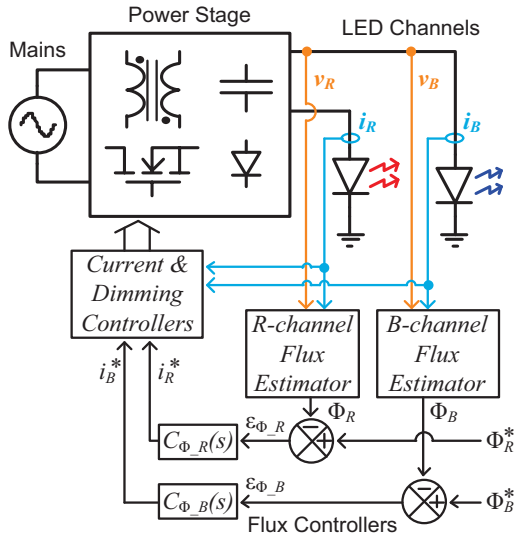

Fig. 6. Overall topology of the two-channel LED driver on development, with inner current and outer flux control loops.

More specifically, on the current driver on development, the power stage is composed of a two-output flyback converter operating in DCM, such that high power factor can be attained [22] and the outputs behave as current sources [23]. The dimming on each channel can be achieved by the use of series transistors operating under PWM [24].

The flux estimators on Fig. 6, as mentioned in the previous section, are simply calculations from equations (2) and (3) from the measured values of v_x and i_x plus previously knowledge of both channels parameters (from Table I).

B. Validation of Flux Estimation

The methodology assumed to validate the flux estimation was accomplished through comparison with radiant flux measurement emulated for four current levels (250, 350, 500 and 750 mA) with a prototype named as "Block". The Block consists in 1/6 part of the luminaire module, three red to one blue, as showed in Fig. 3. It was placed on a metalcore surface and attached in a heatsink with a known thermal equivalent resistance (R_{th_hs}) of 11.32 °C/W.

The real radiant flux was measured with an Integrated Sphere, LMS400 by Labsphere, whereas the estimated radiant flux for each current were calculated from eq. (3) showed in chapter II, section B.

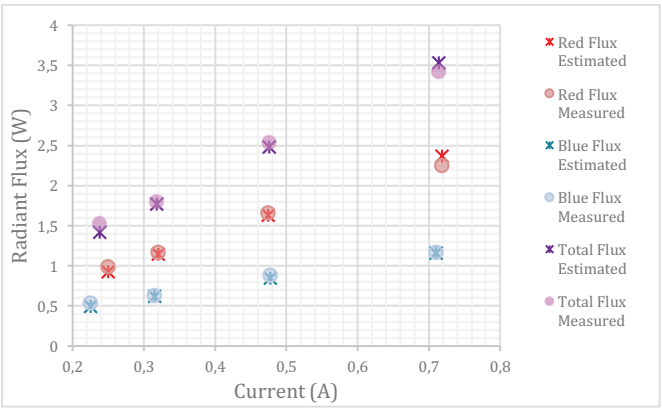

Fig. 7. Comparison of measured and estimated radiant flux for each channel and for total Block flux.

C. Dynamical Model of the Driver for Control Purposes

The dynamical model for the system is composed of the two inner current loops plus the two outer flux loops, totaling the need of 4 describing transfer functions relating the voltages and currents on the output of each channel to the duty-cycle (d) of the flyback converter. Four controllers are also needed: two current controllers and two flux controllers. This is schematically shown in Fig. 8.

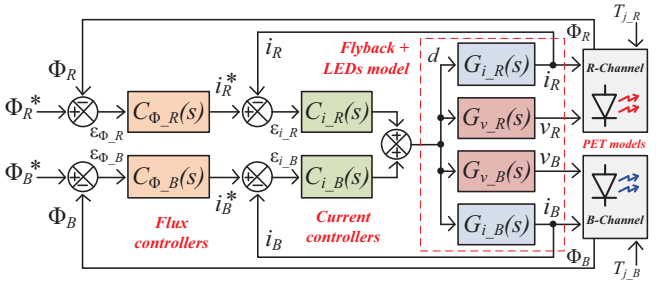

Fig. 8. Block diagram of the control model for all the four loops in the 2-channel driver with flux control under development.

The estimated flux calculated from eq. (2) and eq. (3) is compared with the selected flux reference. If differs, an integrator compensates it and generates the channel reference current. Next, it is compared with measured current and compensate the error with a Proportional-Integral controller. The sum of compensated error from both channels is compared with the modulation carrier frequency of 40 kHz to generate the PWM of the flyback interrupter.

D. Simulation Results of the Driving System

The waveforms in Fig. 9 show the overall workings of the indirect flux control of the proposed driver.

This simulation comprises 300 seconds, and was done using the thermo-electrical circuit of the two LED channels (Fig. 4), each of them being fed by a controlled current source whose control inputs is the calculated current reference on each, i_R* and i_B*. This is equivalent to the averaged model of the DCM flyback driver designed. A small equivalent thermal capacity of 30 J/K for the heatsink was used to speed up the simulation while allows to observe the dynamic of the flux control on the current references for the thermally-interlocked R+B channels. The heatsink thermal resistance is 1.2 K/W. The flux controllers used are simple unitary integrators.

The simulation shows the response of the system for two reference steps – a): at 100 s, B-channel flux reference (superposed in gray) is stepped up from 80% to 100%; at 200 s, R-channel flux reference (also superposed in gray) is stepped down from 100% to 40%. The temperature – b) (calculated by the flux estimator, in gray, and measured in the thermal circuit) in both single-junctions and heatsink rises and falls accordingly, while current in each channel – c) is regulated on real time to maintain the reference flux level. In d), the electrical power delivered to each channel is shown. Because there are more R-LEDs than B-LEDs, they represent a greater share on electrical power. One can also notice that while heatsink temperature rises or falls (during transients), channel currents are also slightly increased or decreased accordingly to maintain their respective flux at the setpoint.

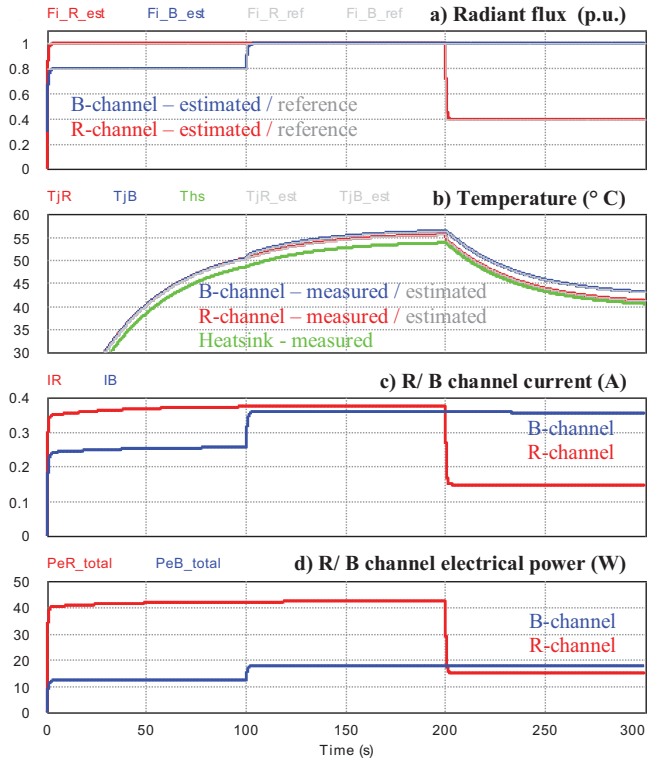

Fig. 9. Simulation of the flux control and driving of both channels represented by their equivalent PET circuit, with control acting from flux estimators.

The waveforms in Fig. 10 show the overall workings simulation of the two-output flyback converter chosen to supply each luminaire.

The simulation total time comprises 0.6 seconds and it is based on radiant flux data of Fig. 7 in order to compare, for each channel, the system dynamic with the expected flux and current measured beforehand.

The simulation starts with a reference radiant flux of 0.99 W and 1.17 W in the channel red and blue, respectively. The drive takes approximately 100 ms to converge to reference and the average current of 0.25 A, for red channel, and 0.71 A, for blue channel is in accordance with the data in Fig. 7. At 0.2 second of simulation, it was inserted a new reference for both channels, 2.251 W for red channel and 0.535 W to blue channel. Again, the controller acts driving the current according the estimated radiant flux for each channel. At 0.4, it was inserted an increment of 10% of the peak input voltage to test the controllability of the circuit under input disturbances.

The first screen of Fig. 10 shows the duty-cycle of flyback interrupter (Dfly) and the input current of the circuit (I(Lf)). The flyback duty-cycle was limited to 0.69 to guarantee DCM operation and the input current shape evidences that the converter operates in a high power factor (0.98).

The second screen shows the duty-cycle of the blue channel and red channel interrupters (D_DimR and D_DimB, respectively). This screen displays the control response for each reference set.

The third screen shows the current for red and blue channels (ILED_R and ILED_B). The dimming occurs in PWM mode, varying the duty-cycle to achieve the average current reference for each channel. This method deployment guarantee less chromatic deviation [25].

The fourth screen shows the radiant flux references (FI_R_ref and FI_B_ref) and the R+B fluxes (FI_R_est and FI_B_est) resulted from the estimator and controllability dynamic of the converter. In sum, this screen evidences that the system is driven and in accordance with flux referenced.

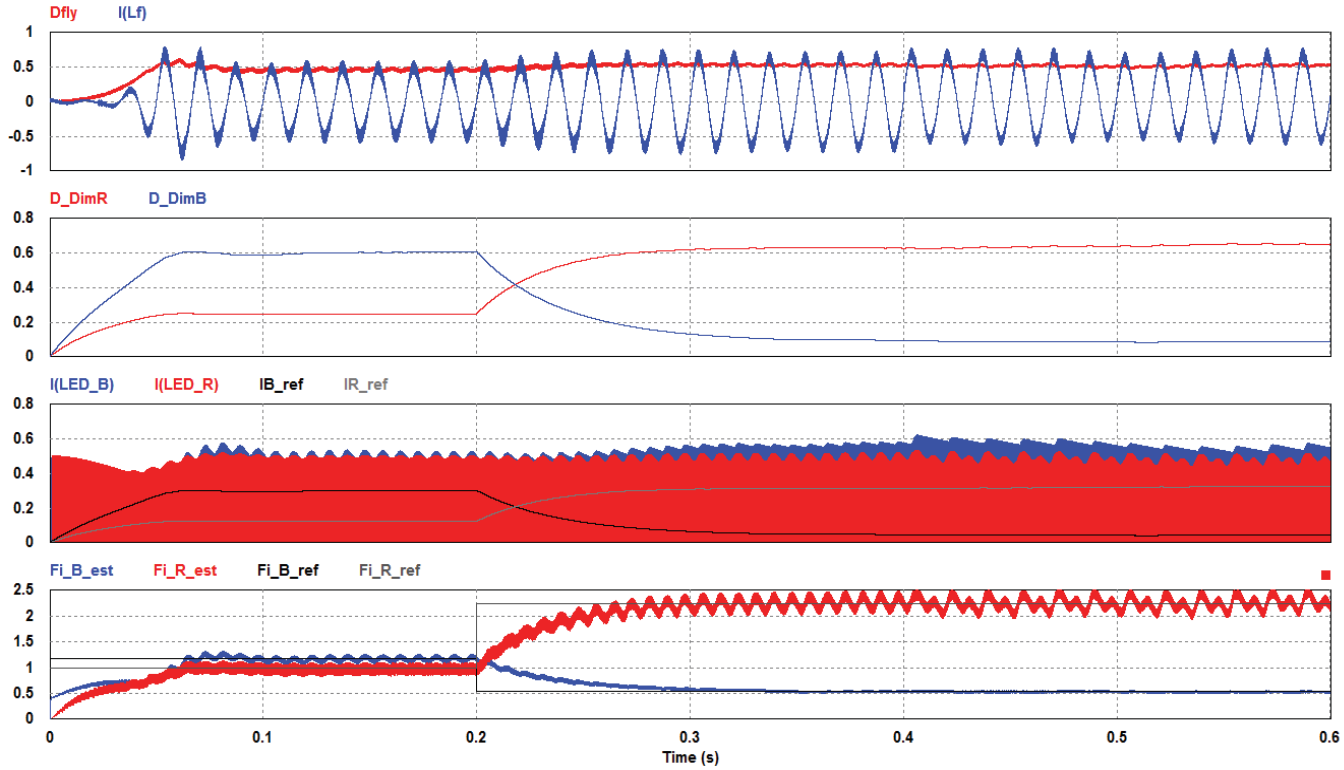

Fig. 10. Simulation of the high power factor DCM flyback converter with independent red and blue channels operating with flux estimation controller.

V. CONCLUSIONS

This paper has presented the PET modeling and proposal of a driver for 2-channel LED system to be deployed in an experiment of greenhouse growing of *H. lupulus*.

Firstly, it was displayed the constraints of the project for indoor horticulture adequacy emphasizing hop cultivation through bibliography contextualization. According to that, it was proposed a specific luminaire designed to attend hops without Sun supplementation, which will be evaluated after further empiric experiments with the plants. Then, the PET model for the two channels was presented and used for estimate the flux of each channel. The radiant flux estimation was validated through comparison with four specific points measured from a segmented prototype of the luminaire (block) in an integrated sphere, as the error of flux is acceptable for controllability. At last, the PET circuit and the flyback converter with estimation control integrated were simulated on PSIM. According to the simulation results, the driver designed presents fair workability to attend the project aims of radiant flux control through an adjustable flux reference.

ACKNOLEDGEMENTS

The authors thank CAPES, CNPq, FAPEMIG, and INERGE for the financial support, the Plant Physiology Department of UFJF for technical support on physiology studies and the availability and support of Hops Brasil Company and Rio Claro Lúpulos to provide the hops seedlings and technical insights needed for the experiment underway.

REFERENCES

[1] B. J. Pearson, R. M. Smith, J. Chen, "Growth, Strobile Yield, and Quality of Four Humulus lupulus Varieties Cultivated in a Protected Open-sided Greenhouse Structure". HortScience, American Society for Horticultural Science, v. 51, 2016.

[2] C. H. Tremblay, and V.J. Tremblay.. "Recent economic developments in the import and craft segment of the US brewing industry".Oxford Univ. Press, Oxford, 2011.

[3] F. P. Prencipe, V. Brighenti, M. Rodolfi, A. Mongelli, C. dall'Asta, T. Ganino, R. Bruni, F. Pellati, "Development of a new high-performance liquid chromatographymethod with diode array and electrospray ionization-massspectrometry detection for the metabolite fingerprinting of bioactivecompounds in Humulus lupulus L.". *Journal of Chromatography A* vol. 1349, pp. 50-59, Italy, 2014.

[4] Z. Kolenc, D. Vodnik, S. Mandelc, B. Javornik, D. Kastelec, A. Cerenak, "Hop (humulus lupulus L.) responses mechanisms in drought stress: Proteomic analysis with physiology". Ljubljana Univ., Ljublijana, Slovenia, March. 18, 2016.

[5] R. Kneen "Small Scale & Organic Hops Production", Left Fields, BC

[6] H. J. Barth, C. Klinke, C. Schmidt, "The hop atlas: The history and geography of the cultivated plant." Joh. Barth & Sohn, Nuremberg, Germany, 1994.

[7] P. PINHO, *"Usage and control of solid-state lighting for plant growth"*. PhD Thesis, Helsinki University of Technology, Espoo, Finland, September 2008.

[8] L. Taiz, E. Zeiger *"Fisiologia Vegetal"*, Artmed, 4ª ed. Porto Alegre, 2009.

[9] Royal Philips N. V. "Philips Horticulture LED Solutions - General booklet", 2015. [Online]. Disponível: www.philips.com/horti.

[10] Nelson, J. A., and Bugbee B. "Economic analysis of greenhouse lighting: light emitting diodes vs. high intensity discharge fixtures." *PLoS One*9.6 (2014): e99010.

[11] K. J. McCree "The Action Spectrum, Absorptance and Quantum Yield of Photosynthesis in Crop Plants", Agricultural Meteorology, n. 8, 191-216, 1971.

[12] OPUS (Pacific) Company Limited, "Hydroponics Plant Grow LED Light", Chai Wan, Hong Kong, 2014. [Online]. Disponível: www.oplusled.com/diymodule.

[13] "What are the best grow lights? Well… that depends. How to choose the perfect LED light for growing Cannabis". [Online]. Disponível: www.ledgrowlights depot.com.

[14] American Society for Testing and Materials (ASTM) Terrestrial Reference Spectra for Photovoltaic Performance Evaluation "Reference Solar Spectral Irradiance: ASTM G-173", 2003. [Online]. Disponível: www.nrel.gov/rredc.

[15] E. D. Freitas, "Agrometeorologia", Departamento de Ciencias Atmosfericas, Instituto Astronomico e Geofísico, Universodade de São Paulo - USP, São Paulo, February 2005.

[16] S. Y. Hui, Y. X. Qin, "A General Photo-Electro-Thermal Theory for Light Emitting Diode (LED) Systems", *IEEE Transactions on Industry Applications*, vol. 24, nº 8, pp. 1967-1976, August 2009.

[17] V. C. Bender, "Metodologia de Projeto Eletrotermico de LEDs Alpicada ao Desenvolvimento de Sistemas de Iluminacao Pública", Universidade Federal de Santa Maria (UFSM), Santa Maria, Brazil, 2012.

[18] V. C. Bender, "Design Methodology for Light-Emitting Diode Systems by Considering an Electrothermal Model", *IEEE Transactions on Electron Devices*, vol. 60, nº 11, November 2013.

[19] P. S. Almeida, "Síntese de Conversores Ressonantes com Alto Fator de Potência e Alta Eficiência para o Acionamento de Diodos Emissores de Luz", PhD Thesis, Universidade Federal de Juiz de Fora (UFJF), Juiz de Fora, Brazil, 2014.

[20] OSRAM Opto Semiconductors, "OSLON SSL 120 GH CSSPM1.24", datasheet, v1.1, 2016.

[21] OSRAM Opto Semiconductors, "OSLON SSL 120 GD CSSPM1.14", datasheet, v1.0, 2016.

[22] X. Xie, J. W. C. Zhao, Q. Lu, S. Liu, "A Novel Output Current Estimation and Regulation Circuit for Primary Side Controlled High Power Factor Single-Stage Flyback LED Driver", *IEEE Transactions on Power Electronics*, v.27, n. 11, 2012.

[23] D. Gacio, J. M. Alonso, J. Garcia, D. G.Llera, J. Cardesin, "Optimization of a Front-End DCM Buck PFP for an HPF Integrated Single-Stage LED Driver",

Journal of Emerging and Selected Topics on Power Electronics, v.3, n. 3, 2015.

[24] D. Gacio, J. M. Alonso, J. Garcia, L. Campa, M. J. Crespo, M. Rico-Secades, "PWM Series Dimming for Slow-Dynamics HPF LED Drivers: the High-Frequency Approach", *IEEE Transactions on Industrial Electronics*, v. 59, n. 4, 2012

[25] P. S. Almeida, F. J. Nogueira, L. F. A. Guedes and H. A. C. Braga, "An Experimental Study on the Photometrical Impacts of Several Current Waveforms on Power White LEDs," *XI Brazilian Power Electronics Conference*, Praiamar, 2011, pp. 728-733.